Numerical Simulation of Growth and Departure Behavior of Vapor Bubble in Flow Boling

Zuzhi Li[a], Jonghwi Choi, Hyungdae Kim [*]

Department of Nuclear Engineering, Kyung Hee University, Yongin-si, Republic of Korea

*Corresponding Author: hdkims@khu.ac.kr

*Keywords: Numerical Simulation, Interface Tracking, Single Bubble, Microlayer, Flow Boling

1. Introduction

Two-phase flow heat transfer including phase change phenomenon within the nuclear power plant is critical for predicting time and space resolved the surface temperature and heat flux at fuel cladding. To investigate such effects through Computational Fluid Dynamics (CFD) tools, the microlayer which is a very thin liquid layer exist beneath of the bubble's base [1] was considered as a wall function implemented in wall adjacent cells, shown in Fig.1. To better depict the interface between a heated wall and boiling bubbles, solving the conjugated heat transfer problem is considered. Also, for the macroscopic region, the interfacial tracking method [2] was applied to capture the bubble's interface. In this paper, a series of systemic simulations has been operated to investigate the variation of bubble's size and related wall temperature based on different pressure and flowing conditions,

The aim of this study is to figure out the how system pressure and flow conditions affect the bubble's growth and departure characteristics.
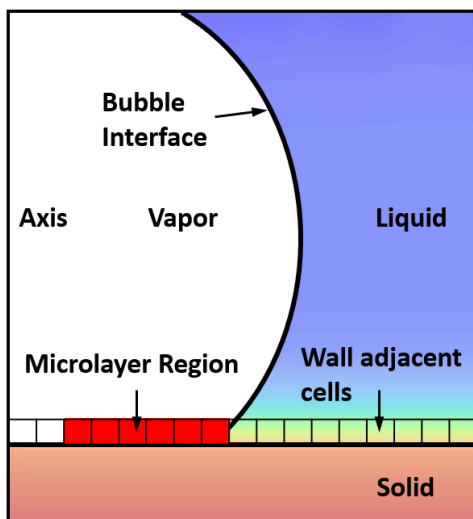
Fig. 1 The implementation of microlayer model.
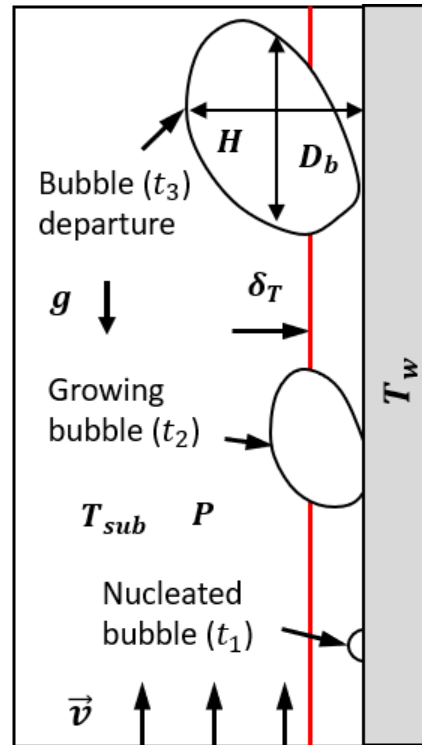
Fig. 2 The Schematic illustration of Problem Set.

Fig. 2 schematically shows the bubble states at different moments, nucleation (t_1), growth (t_2) and departure (t_3) [3]. Firstly, the nucleated bubble will be initialized inside of the thermal boundary layer δ_T with subcooling T_{sub} conditions in background. By altering the velocity of inlet flow $\vec{v}$ and ambient pressure P, the bubble will display distinct departure dimeter D_b and departure height H. Also, gravity is set to against the flow velocity. In this paper, we will record this variation as a function of time to try to get the insight behind the phenomenon.

2. Numerical Methods

2.1 Governing Equations

The equations that need to be considered for simulation are as follows: the equations of volume fraction, momentum and energy conservation, respectively. It is worthy mention that the conjugated heat transfer is considered in computational domain, therefore the energy governing equation is distinct from the liquid cells and solid cells. The boundary conditions for coupled wall are given in Eq.5 [4].

$$\frac{\partial \alpha_v}{\partial t} + \nabla \cdot (\vec{v} \cdot \alpha_v) = \frac{S_{tot}}{\rho} \tag{1}$$

$$\frac{\partial \rho \vec{u}}{\partial t} + \nabla \cdot (\vec{u} \cdot \rho \vec{u}) = -\nabla \cdot p + \nabla(\mu \nabla \vec{u}) + F_g + F_{sur} \tag{2}$$

For liquid cells:

$$\frac{\partial \rho U_l}{\partial t} + \nabla \cdot (u \cdot \rho U_l) = \nabla \cdot \left(\lambda_{eff} \cdot \nabla T\right) + S_{h,l} \tag{3}$$

For solid cells:

$$\frac{\partial \rho U_s}{\partial t} = \nabla \cdot (\lambda_s \cdot \nabla T) \tag{4}$$

The boundary condition at the liquid-solid interface:

$$q'' = k_{eff} \frac{\partial T}{\partial n}\bigg|_l = -k_s \frac{\partial T}{\partial n}\bigg|_s \tag{5}$$

S_{tot} is the mass source term applied in liquid cells including the interfacial source term and microlayer source term, ρ is the density, $\vec{v}$ is velocity. F_g is the gravity, F_{sur} is the surface tension force. $S_{h,l}$ is the negative energy source term for liquid cells. λ_{eff} is the effective heat transfer coefficient for microlayer cells. λ_s is the heat transfer coefficient for solid cells. U_l is internal energy, which the product of temperature and heat capacity. For equations in above the subscript with l means the heat flux at liquid side whereas the s means the heat flux at solid side.

2.2 Surface tension force

To account for the effects of surface tension in CFD, the Volume of Fluid (VOF) method with the Continuum Surface Force (CSF) model [5] has been adopted. In the CSF model, the surface tension of the bubbles can be expressed as volumetric forces using the divergence theorem. The equation for this can be formulated as follows:

$$F_s = \sigma \frac{\alpha_l \rho_l \kappa_v \nabla \alpha_v + \alpha_v \rho_v \kappa_l \nabla \alpha_l}{\frac{1}{2}(\rho_l + \rho_v)} \tag{6}$$

$$n_f = \nabla \alpha_l, n_v = \nabla \alpha_l \tag{7}$$

$$\vec{n} = \frac{n}{|n|} \tag{8}$$

$$\kappa_l = \nabla \cdot \overrightarrow{n_l}, \kappa_v = \nabla \cdot \overrightarrow{n_v} \tag{9}$$

ρ represents density. σ is the surface tension coefficient. α is the volume fraction in the control volume. n stands for the surface normal. denotes curvature, which is expressed as the divergence of the gradient of α. l and v represent the liquid and vapor phases, respectively. This model is very crucial to reconstruct the bubble interface, especially when it comes to behavior of multiphase flow.

2.3 Evaporation model

In this section, we will discuss the detail evaporation model which was implemented in simulation, involving the interfacial evaporation model and microlayer evaporation model.

2.3.1 Interfacial Evaporation Model

In the analysis of the growth of individual bubbles, heat transfer at the vapor-liquid interface is modeled using Lee's phase change model. Lee's phase change model (referred to as the Lee model) assumes phase change occurs under constant pressure and quasi-thermodynamic equilibrium conditions. In the Lee model, evaporation and condensation are induced by the vapor transport equation [6]. This approach is used to describe the mechanisms of heat and mass transfer during the growth of bubbles, especially focusing on phase change phenomena, and it provides insight into the intricate dynamics of the process.

$$\dot{m}_{lv} = \Omega * \alpha_l \rho_l \frac{T - T_{sat}}{T_{sat}} \quad for\ T > T_{sat} \tag{10}$$

$$\dot{m}_{vl} = \Omega * \alpha_v \rho_v \frac{T - T_{sat}}{T_{sat}} \quad for\ T < T_{sat} \tag{11}$$

The energy source term related to the equation is obtained by multiplying the latent heat h_{lv} to Eq. 13 and 14.

$$S_{h,lv} = -\dot{m}_{lv} \times h_{lv} \tag{12}$$

The larger the value of coefficient Ω, the more intense the heat and mass transfer at the phase interface is, and the closer the interface temperature is to the saturation temperature. However, too large value of coefficient can lead to unstable interface morphology or even break up. Therefore, in this study the coefficient $\Omega = 6000$.

2.3.2 Microlayer Evaporation Model

When it comes to discuss the boiling phenomenon, microlayer evaporation is a very critical heat transfer mechanism [7]. The importance of microlayer is attributed to the extremely high temperature gradient inside the layer, causing the very huge heat flux with dramatic phase change. Once the microlayer format, it will arise a series of chain reactions and coupled relationships between microlayer thickens, wall temperature and wall heat flux [8], seen in Fig. 3. Such phenomenon can be explained as: the dramatic phase change existing inside of microlayer will decrease the temperature of the wall and thinner the thickness of microlayer. Therefore, the temperature gradient become larger, so the heat flux also become higher, phase change become more dramatic. Such chain reactions will keep existing until the microlayer is fully depleted. That can also explain why the wall temperature is higher whereas the heat flux is lower for the area that without microlayer. Because there is no microlayer to drive dramatic phase change.
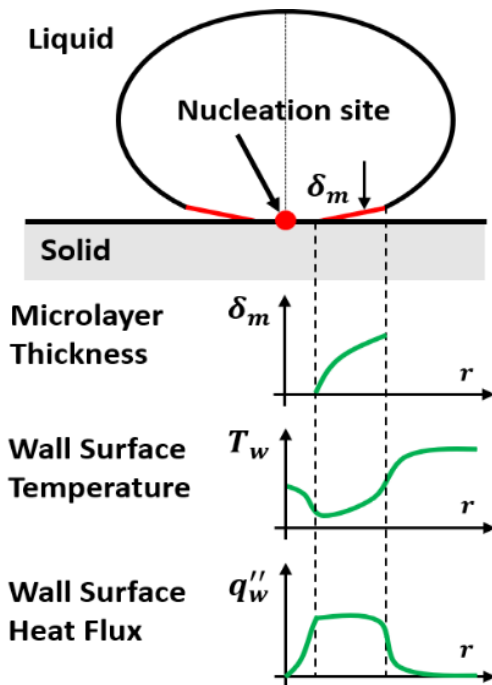
Fig. 3 Coupled relation between microlayer thickness, wall temperature and wall heat flux.

The heat flux through the microlayer can be expressed as:

$$q_m'' = \left(\frac{T_w - T_{sat}}{h_{ev} + \delta_m/\lambda_l} \right) \tag{13}$$

T_w is the wall temperature, h_{ev} is the evaporative thermal resistance, δ_m is the microlayer thickness, λ_l is the thermal conductivity of liquid.

Phase change rate followed the expression in below, it can be simply interpreted as the heat flux divided by latent heat:

$$M_m = q_m''/L \tag{14}$$

If the bubble expands to new area, a micro-layer of initial thickness δ_0 is added to the expanded area, with initial thickness expressed as:

$$\delta_0 = C \times r_0{}^{0.69} \tag{15}$$

The coefficient C is taken as 0.0046 which is recommended by the Sato's study [9], where the microlayer depleted model was proposed. This study follows quiet similar technique by writing the User define functions in Fluent.

To simulate the depletion of microlayer thickness, an explicit method is employed for the time discretization:

$$\frac{\delta^{n-1} - \delta^n}{\Delta t} = \frac{1}{\rho_l} M_m^n \tag{16}$$

The superscript "n" and "$n-1$" represent the previous time step and current time step, respectively. Δt represent the time step of the simulation which is taken as $10^{-6} s$ to insure the convergence.

To avoid the infinite small value exits in microlayer thickness, we have limitations:

$$\text{If } \delta^n < 1.0 \times 10^{-10} m, \text{ set } S_m \equiv 0 \tag{17}$$

The energy source related with microlayer evaporation has quite similar formation with interfacial evaporation, which can be expressed by:

$$S_{h,m} = -M_m^n \times h_{lv} \tag{18}$$

Therefore, the total mass transfer is the summation of microlayer source and interfacial source:

$$S_{tot} = M_m + \dot{m}_{lv} + \dot{m}_{vl} \qquad (19)$$

Also, the total energy source is the summation of microlayer energy source term and interfacial source term:

$$S_{h,tot} = S_{h,m} + S_{h,lv} \qquad (20)$$

3. Computational Setup and Boundary Conditions

As we illustrated before, the conjugated heat transfer will be investigated in simulation, therefore, it is clear that the solid domain has been displayed in Fig.4. At the very bottom of the simulation domain the heat flux is applied with the fixed value of $53\ KW/m^2$ and $1000\ KW/m^2$. The contact angle of bubble is set as $20°$. To generate the thermal boundary, the preheating time is about 2s. With these initial conations, the bubble seed is patched with the radius of 0.05mm which is also the mesh size in this simulation. The length of the simulation domain is 10mm with the width of 5.5mm. The subcooling temperature is set as 1 K for all of the cases.
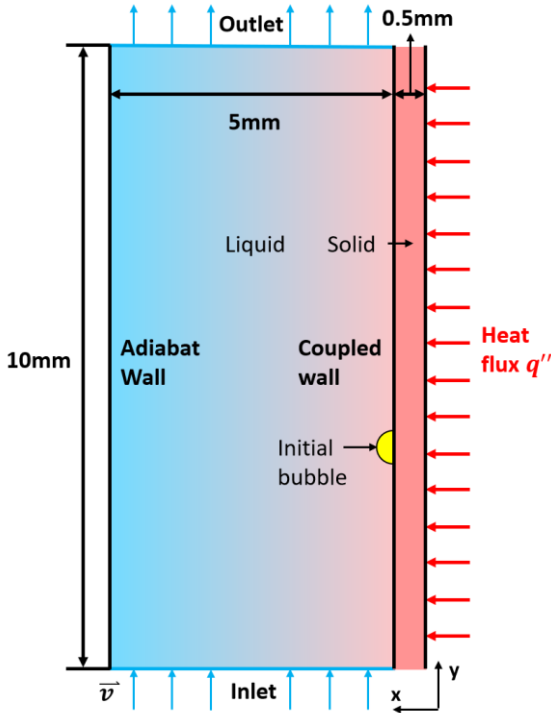
Fig. 4 Simulation domain and mesh distribution

The table in blow shows the pressure conditions and flowing conditions for different cases.

Table.1 The test boundary conditions for different cases

	Case Number			
	1	2	3	4
Pressure (MPa)	0.1	0.1	7	15
Bulk Velocity (m/s)	0.1	0.3	2	2
Heat flux (kw/m^2)	53	53	1000	1000

For different pressure flowing conditions, the material property at its saturated temperature is also different. The Table.2 [10] displayed the material properties of working fluid vapor, liquid under different pressure. Here, we assume the material property of Zr Alloy remains constant.

Table.2 The property of working fluid under different pressure and Zr alloy

Material	P [MPa]	ρ $[kg/m^3]$	c_p $[J/(kg \cdot K)]$
Vapor	0.1	0.597	2080
	0.8	3.644	2310
	1.5	4.147	2520
Liquid	0.1	958.4	4220
	0.8	922.8	4380
	1.5	926.6	4310
Zr Alloy	Null	652	270

	λ $[W/(m \cdot K)]$	ν $[kg/(m \cdot s)]$	σ (N/m)
Vapor	0.0254	1.3×10^{-5}	0.059
	0.0266	1.77×10^{-5}	0.589
	0.0321	1.92×10^{-5}	0.549
Liquid	0.672	2.8×10^{-4}	0.059

	0.675	1.6×10^{-4}	0.589
	0.679	1.2×10^{-4}	0.549
Zr Alloy	22	Null	Null

To investigate the behavior of individual bubble growth, the VOF method in ANSYS FLUENT 2022 R2 is employed for analysis. In consideration of surface tension during bubble growth, the CSF model is applied in the simulation. Various source terms are implemented in the simulation using UDFs [11]. To ensure the simulation has good convergence, the criterion for convergence was set as 10^{-8} for energy governing equation and 10^{-6} for the other equations. Additionally, to allow sufficient observation of bubble growth until detachment from the heating surface, the number of time steps is set to 20000.

4. Results and Discussion

The temperature contour is given in below Fig. 5. It can be observed the temperature drop in the solid phase. Also, the volume fraction contour is displayed in below. For case 1 and case 2, it is apparent that with the increase of the bulk velocity, the bubble size become smaller. The dominate reasons can be explained as, faster bulk velocity will remove more sensible heat of the solid surface, therefore the wall temperature will be small, the thickness of thermal boundary layer will thinner. So, the phase change rate will be less dramatic causing the size of bubble be smaller. The data of bubble diameter and bubble height was drawn in Fig. 6, through this plot, such phenomenon will be more clearly observed.

Case 1
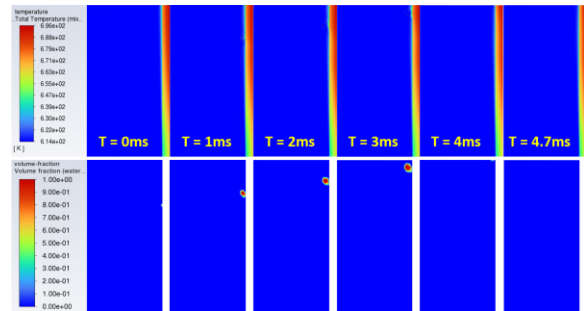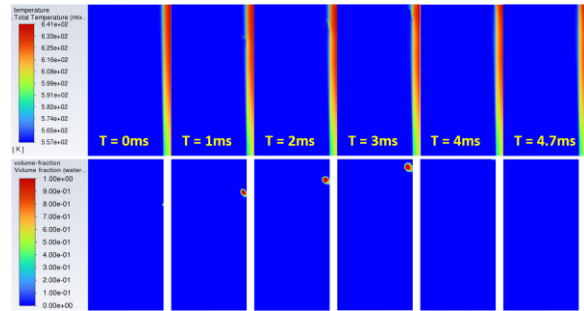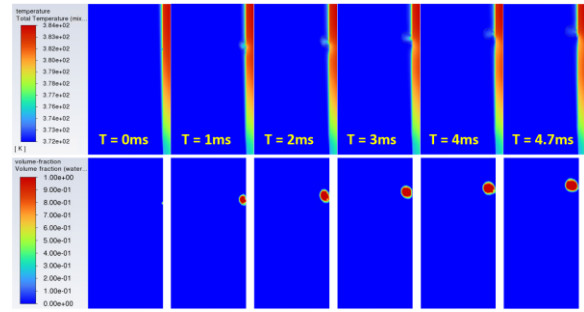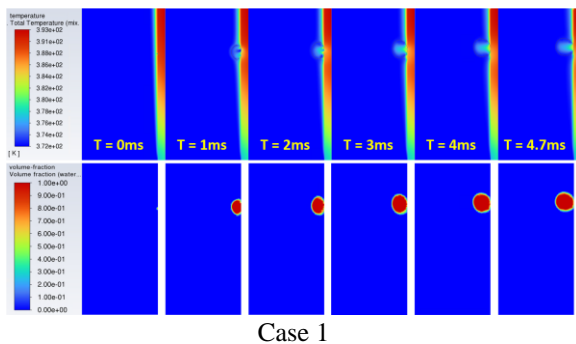
Case 2

Case 3

Case 4

Fig. 5 The temperature distribution and volume fraction for case 1, case 2, case 3 and case 4 respectively

For case 3 and case 4, the influence which aroused by the pressure seems very trivial. It is hard to directly to recognize the distinguish between case 3 and case 4 through eyes. Fortunately, Fig. 7 provided a clearer view about the how the pressure affects the bubble's size. As the ambient pressure increase, the bubble size will be smaller. Such phenomenon is attributed to the effect of more feasible compressibility of the vapor. When, the ambient pressure is higher, the bubble will be pressed smaller.
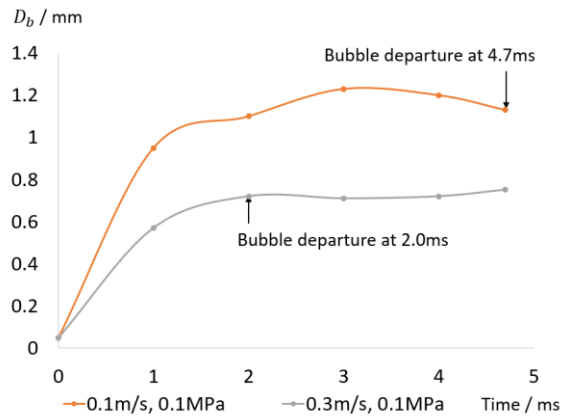
Fig. 6 Effect of bulk velocity on bubble diameter
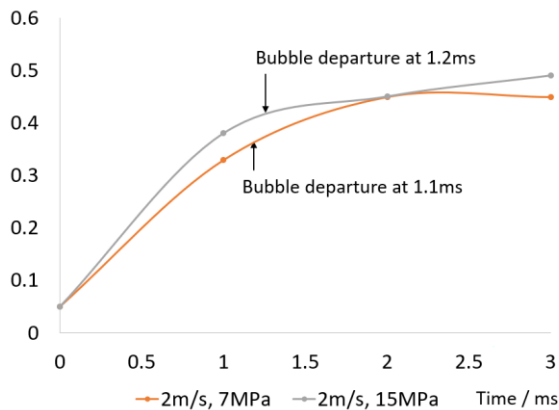
Fig. 7 Effect of system pressure on bubble diameter

5. Conclusion

Based on above phenomenon given by case 1 and case 2, it is clear that as the bulk velocity decrease, the bubble's size including the diameter and height increase. Also, the bubble departure time and bubble departure diameter will delay if the bulk velocity is lower. From the view of case 3 and case 4, if the system pressure is higher, it will be observed that an early bubble departure with relatively smaller bubble's size.

It is worthy to mention that while the surface conditions including the surface roughness mainly affect nucleation site density, this preliminary study is limited to single bubble boiling from one predetermined site. We will expand this study toward multi-bubble conditions later.

The boundary conditions, especially the heat flux in this simulation, is too large comparing with that in PWR. Therefore, the further investigation about the influence of heat flux will be done in future.

7. Reference

[1] S. Jung and H. Kim, "Hydrodynamic formation of a microlayer underneath a boiling bubble," Int. J. Heat Mass Transfer 120, 1229–1240 (2018).
[2] C. W. Hirt and B. D. Nichols, "Volume of fluid (VOF) method for the dynamics of free boundaries," J. Compute. Phys. 39(1), 201–225 (1981).
[3] G. Sinha, S. Narayan and A. Srivastava, "Microlayer dynamics during the growth process of a single vapor bubble under subcooled flow boiling conditions" J. Fluid Mech. (2022), vol. 931, A23, doi:10.1017/jfm.2021.95
[4] Computational Fluid Dynamics the Finite Volume Method, Chapter Eight the Finite Volume Method for unsteady flows, pp.243-266
[5] J. U. Brackbill, D. B. Kothe, and C. Zemach, "A continuum method for modeling surface tension," J. Compute. Phys. 100(2), 335–354 (1992)
[6] W.H. Lee, A pressure iteration scheme for two-phase flow modeling, in: Computational Methods for Two-phase Flow and Particle Transport, 1980, pp. 61–82.
[7] Z.H. Chen, X.H. Hua, K, Hua, Y, S. Utaka, S.J. Mori, Measurement of the microlayer characteristics in the whole range of nucleate boiling for water by laser interferometry, International Journal of Heat and Mass Transfer 146 (2020) 118856
[8] Jung, S., Kim, H., 2014. An experimental method to simultaneously measure the dynamics and heat transfer associated with a single bubble during nucleate boiling on a horizontal surface. Int. J. Heat Mass Transf. 73, 365–375.
[9] Y. Sato, B. Niceno, A depletable micro-layer model for nucleate pool boiling, J. Compute. Phys. 300 (2015) 20–52.
[10] Steam Table, DOI: 10.1615/AtoZ.s.steam_tables.
[11] Ansys Fluent UDF Manual, Ansys, Inc, Release 15.0 (2013)